

Technical Note

Transient dynamic response of a shallow buried lined tunnel in saturated soil



Y. Wang^a, G.Y. Gao^{b,*}, J. Yang^c, X.Y. Bai^d

^a Institute of Civil Engineering and Architecture, Qingdao Binhai University, Qingdao 266555, China

^b Key Laboratory of Geotechnical and Underground Engineering of Ministry of Education, Tongji University, Shanghai 200092, China

^c Department of Civil Engineering, The University of Hong Kong, Hong Kong, China

^d Department of Civil, Environmental & Architectural Engineering, University of Colorado, Boulder, CO 80302, USA

ARTICLE INFO

Keywords:

Transient dynamic response
Lined tunnel
Half space
Saturated soil
Laplace transform

ABSTRACT

Previous research has produced valuable results on the transient dynamic response of tunnels buried in full-space. However, a half-space model is of more practical interest because tunnels normally have finite buried depths. In this paper, the dynamic response of a lined tunnel is studied where the surrounding soil is described using Biot's theory and the lining is described by the theory of elastodynamics. The half-space straight boundary is approximately represented by a convex arc of large radius. In accordance with Graff's addition theorem, the general solutions in a rectangular coordinate system are converted to ones in a polar coordinate system. The solutions for displacements and stresses of both the soil and the lining as well as the pore pressure of the soil in the Laplace transform domain are derived based on boundary conditions. Time domain solutions are then obtained by the use of inverse Laplace transform. Numerical results are presented showing the distributions of peak values of ground displacements, stresses and pore pressures of the soil.

1. Introduction

Underground lined structures are sometimes subjected to transient dynamic loadings such as hydraulic fracture initiation, blasting loading and sudden excavations, which can be simplified as a suddenly applied constant load, a gradually applied step load or a triangular pulse load. These transient loadings may cause failure of the underground structures and their surrounding soil. Therefore it is very important to investigate the stress and displacement of the lined structure and the soil under the transient loadings.

Previous research has produced valuable results on the transient dynamic response of underground structures. Senjuntichai and Rajapakse [1] obtained transient solutions of a long cylindrical cavity induced by a suddenly applied constant load, a gradually applied step load and a triangular pulse load. The cavity was assumed to be buried in an infinite poroelastic medium and not to be lined. Kattis et al. [2] obtained numerical solutions for dynamic response of both the unlined and lined tunnels in an infinite poroelastic saturated soil under a harmonic wave diffraction by the boundary element method. Xie et al. [3] studied dynamic response of a partially sealed circular tunnel in viscoelastic saturated soil. Osinov [4] investigated the dynamic response of saturated granular soil induced by a blast loading on a tunnel

lining. Gao et al. [5] obtained an analytical solution for transient response of a cylindrical lined cavity in a poroelastic medium. Wang et al. [6] investigated the influence of the degree of saturation on dynamic response of a cylindrical lined cavity in a nearly saturated poroelastic medium. Gao et al. [7] presented an exact solution for three-dimensional dynamic response of a cylindrical lined tunnel in saturated soil to an internal blast loading. All of these studies assumed the tunnel to be buried in a full-space, whereas a half-space model apparently is of more practical because tunnels always have finite buried depths.

In this paper, the governing equations of the soil surrounding a lined tunnel are given based on Biot's theory in a rectangular coordinate system, and the governing equations of the lining are presented based on the conventional theory of elastodynamics. The general dynamic solutions of both the surrounding soil and the lining are then obtained by the use of Laplace transform. A large radius arch is used to approximately represent the free surface boundary of the half-space. Then the general solutions in the rectangular coordinate system are transformed into solutions in the polar coordinate system by applying Graff's addition theorem [8]. By matching boundary conditions, the special solutions are derived. The peak value of ground displacement, hoop stress in the lining and pore pressure distribution

* Correspondence to: College of Civil Engineering, Tongji University, Shanghai 200092, China.
E-mail address: gaoguangyun@263.net (G.Y. Gao).

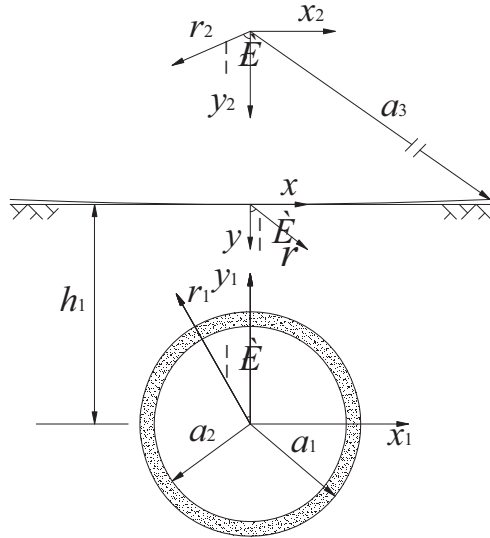


Fig. 1. Analytical model and straight boundary in the half space model.

between the lining and the surrounding soil in time domain are obtained by numerical inverse Laplace transform.

2. Governing equations

As shown in Fig. 1, a circular tunnel with infinite length is buried at the depth of h_1 in a saturated half-space. The outer and inner radii of the tunnel are a_1 and a_2 , respectively. The inner surface of the lining is subjected to three types of transient loading (see Ref. [5]).

Treating the soil as a fluid-saturated poroelastic medium, the equilibrium equations of soil skeleton and the fluid are as follows:

$$(\lambda_s + \alpha^2 M + G_s)u_{j,ji} + G_s u_{i,jj} + \alpha M w_{j,ji} = \rho \ddot{u}_i + \rho_f \dot{w}_i \quad i, j = x, y \quad (1)$$

$$\alpha M u_{i,ji} + M w_{j,ji} = \rho_f \ddot{u}_i + \rho_m \dot{w}_i + b \dot{w}_i \quad i, j = x, y \quad (2)$$

where λ_s and G_s are Lamé constants of the saturated soil; α and M are the Biot's coefficients; u_i and w_i are the displacement of the soil skeleton and the displacement of the fluid relative to the solid; ρ is the mass density of saturated soil, $\rho = (1 - n_f)\rho_s + n_f \rho_f$, n_f is porosity of soils, ρ_f and ρ_s are respectively the mass density of pore fluid and solid skeleton; b is the fluid viscous coupling coefficient; ρ_m is the fluid additional mass density, $\rho_m = (n_f \rho_f + \rho_a) / n_f^2$, ρ_a is the mass density induced by fluid coupling.

By introducing potential functions :

$$u_i = \varphi_{1,i} + e_{ijk} \psi_{1k,j}, \quad w_i = \varphi_{2,i} + e_{ijk} \psi_{2k,j} \quad (3)$$

where $\varphi_1(r_1, \theta_1)$, $\psi_1(r_1, \theta_1)$ and $\varphi_2(r_1, \theta_1)$, $\psi_2(r_1, \theta_1)$ are the potential functions of soil skeleton and the fluid, respectively; e_{ijk} is the permutation tensor in rectangular coordinates.

Substituting Eq. (3) into Eqs. (1) and (2), the equilibrium equations as follows:

$$(\lambda_s + \alpha^2 M + 2G_s)\varphi_{1,ijj} + e_{ijk}\psi_{1k,ijj} + \alpha M\varphi_{2,ijj} = \rho(\ddot{\varphi}_{1,i} + e_{ijk}\psi_{1k,j}) + \rho_f(\ddot{\varphi}_{2,i} + e_{ijk}\psi_{2k,j}) \quad (4)$$

$$\alpha M\varphi_{1,ijj} + M\varphi_{2,ijj} = \rho_f(\ddot{\varphi}_{1,i} + e_{ijk}\psi_{1k,j}) + m(\ddot{\varphi}_{2,i} + e_{ijk}\psi_{2k,j}) + b(\dot{\varphi}_{2,i} + e_{ijk}\psi_{2k,j}) \quad (5)$$

Applying Laplace transform to both sides of Eqs. (4) and (5), denoting $\bar{\varphi}_1 = L[\varphi_1]$, $\bar{\varphi}_2 = L[\varphi_2]$, $\bar{\psi}_1 = L[\psi_1]$, $\bar{\psi}_2 = L[\psi_2]$ as the Laplace transform of $\varphi_1(r_1, \theta_1)$, $\varphi_2(r_1, \theta_1)$, $\psi_1(r_1, \theta_1)$, $\psi_2(r_1, \theta_1)$, the governing equations of the soil can be written as (the non-dimensionalized quantities with respect to length and time by selecting the inner radius of the tunnel a_2 as a unit of length and $a_2(\rho/G_s)^{0.5}$ as a unit of time, see

Ref. [5]):

$$(\lambda_c + 2)\nabla^2 \bar{\varphi}_1 + \alpha M^* \bar{\varphi}_2 = s^2 \bar{\varphi}_1 + \rho^* s^2 \bar{\varphi}_2, \quad \alpha M^* \nabla^2 \bar{\varphi}_1 + M^* \bar{\varphi}_2 = \rho^* s^2 \bar{\varphi}_1 + (\rho_m^* s^2 + b^* s) \bar{\varphi}_2 \quad (6)$$

$$\nabla^2 \bar{\psi}_1 = s^2 \bar{\psi}_1 + \rho^* s^2 \bar{\psi}_2, \quad \rho^* s^2 \bar{\psi}_1 + (\rho_m^* s^2 + b^* s) \bar{\psi}_2 = 0 \quad (7)$$

where $\nabla^2 = \frac{\partial^2}{\partial x^2} + \frac{\partial^2}{\partial y^2}$; $\lambda_c = \lambda_s^* + \alpha M^*$; $\lambda_s^* = \frac{\lambda_s}{G_s}$; $M^* = \frac{M}{G_s}$; $\rho^* = \frac{\rho_f}{\rho}$; $\rho_m^* = \frac{\rho_m}{\rho}$; $b^* = \frac{a_2 b}{\sqrt{\rho G_s}}$; $t^* = t / [a_2(\rho/G_s)^{0.5}]$, t is time.

Following the procedures in Gao et al. [5], the general solutions of the governing Eqs. (6)–(7) can be derived as:

$$\bar{\varphi}_1 = B_3(s)I_0(\beta_3 r^*) + B_4(s)K_0(\beta_4 r^*), \quad \bar{\varphi}_2 = C_3(s)I_0(\beta_3 r^*) + C_4(s)K_0(\beta_4 r^*) \quad (8)$$

$$\bar{\psi}_1 = D_5(s)K_0(\beta_5 r^*), \quad \bar{\psi}_2 = m_7 \bar{\psi}_1, \quad m_7 = -(\rho^* s^2) / (\rho_m^* s^2 + b^* s) \quad (9)$$

where $B_3(s)$, $B_4(s)$, $C_3(s)$, $C_4(s)$ and $D_5(s)$ are undetermined coefficients, I_0 and K_0 are the modified Bessel functions of the first and second kinds of order 0, respectively; s is the Laplace transform parameter; β_3 , β_4 , β_5 are the dimensionless wave numbers associated with the two dilatational waves and shear wave, respectively. They can be written as follows:

$$\beta_3^2 = \frac{m_3 + \sqrt{m_3^2 - 4m_4}}{2}, \quad \beta_4^2 = \frac{m_3 - \sqrt{m_3^2 - 4m_4}}{2}, \quad \beta_5^2 = \frac{(\rho_m^* s^2 + b^* s)s^2 - \rho^* s^4}{(\rho_m^* s^2 + b^* s)} \quad (10)$$

$$m_3 = \frac{(\lambda_c + 2)(\rho_m^* s^2 + b^* s) - s^2 M^* + 2\alpha M^* \rho^* s^2}{\lambda_s^* M^* + 2M^*}, \quad m_4 = \frac{(\rho_m^* s^2 + b^* s)s^2 - \rho^* s^4}{\lambda_s^* M^* + 2M^*}, \quad m_7 = -\frac{\rho^* s^2}{(\rho_m^* s^2 + b^* s)} \quad (11)$$

The lining of the cavity is treated as an elastic medium. The governing equations can be obtained as follows by linear elastic wave theory,

$$G u_{i,jj}^L + (\lambda + G) u_{j,ji}^L = \rho_L \ddot{u}_i^L \quad (12)$$

where λ and G are respectively the lining elastic constants; ρ_L is the mass density of the lining; u_i^L and \ddot{u}_i^L are respectively the lining displacement and acceleration.

Similarly, the general solutions of the lining can be written as:

$$\bar{\varphi} = A_6(s)I_0(\beta_6 r^*) + B_6(s)K_0(\beta_6 r^*) \quad (13)$$

$$\bar{\psi} = A_7(s)I_0(\beta_7 r^*) + B_7(s)K_0(\beta_7 r^*) \quad (14)$$

where $A_6(s)$, $A_7(s)$, $B_6(s)$ and $B_7(s)$ are the undetermined coefficients; β_6 , β_7 are the dimensionless wave numbers associated with the compression wave and shear wave and can respectively be expressed as $\beta_6^2 = s^2(c^*)^2$ and $\beta_7^2 = s^2(c_s^*)^2$, in which $(c^*)^2 = (\lambda^* + G^*) / \rho_L^*$, $(c_s^*)^2 = G^* / \rho_L^*$, $\lambda^* = \lambda / G_s$, $G^* = G / G_s$, $\rho_L^* = \rho_L / \rho$. Here c^* and c_s^* are the non-dimensionalized velocity of compression wave and shear wave, respectively.

3. Coordinate transformation

For the half-space straight boundary, the boundary is represented as a convex arc with a large radius a_3 ($a_3 = 6000 a_2$), as shown in Fig. 1.

Using addition theorem by Graff [8], a set of general solutions in the rectangular coordinate system are transformed into solutions in the polar coordinate system:

$$Z_n(\beta r_2) \cos(n\theta_2) = \sum_{m=-\infty}^{\infty} Z_{n+m}(\beta D) J_m(\beta r_1) \cos(n\theta_1), \quad (r_2 < D) \quad (15)$$

where $Z_n(\cdot)$ is the functions of $I_n(\cdot)$ or $K_n(\cdot)$; D is the distance between two origins of the coordinate systems.

By using coordinate transformation, the equations can be expressed as follows in coordinate (r_2, θ_2)

$$\begin{aligned} \bar{\varphi}_1(r_2, \theta_2) &= [J_m(\beta_3 r_2) a_m + J_m(\beta_4 r_2) b_m] \cos m\theta_2, \\ \bar{\varphi}_2(r_2, \theta_2) &= [J_m(\beta_3 r_2) c_m + J_m(\beta_4 r_2) d_m] \cos m\theta_2 \end{aligned} \quad (16a)$$

$$\bar{\psi}_1(r_2, \theta_2) = J_m(\beta_5 r_2) e_m \cos m\theta_2, \quad \bar{\psi}_2(r_2, \theta_2) = m_7 J_m(\beta_5 r_2) e_m \cos m\theta_2 \quad (16b)$$

$$\begin{aligned} \bar{\varphi}(r_2, \theta_2) &= [J_m(\beta_6 r_2) f_m + J_m(\beta_6 r_2) g_m] \cos m\theta_2, \\ \bar{\psi}(r_2, \theta_2) &= [J_m(\beta_7 r_2) h_m + J_m(\beta_7 r_2) i_m] \cos m\theta_2 \end{aligned} \quad (16c)$$

where

$$\begin{aligned} \begin{bmatrix} a_m \\ c_m \end{bmatrix} &= \sum_{n=-\infty}^{\infty} K_{n+m}(\beta_3 D) \begin{bmatrix} B_3(s) \\ C_3(s) \end{bmatrix}; & \begin{bmatrix} b_m \\ d_m \end{bmatrix} &= \sum_{n=-\infty}^{\infty} K_{n+m}(\beta_4 D) \begin{bmatrix} B_4(s) \\ C_4(s) \end{bmatrix}; \\ e_m &= \sum_{n=-\infty}^{\infty} K_{n+m}(\beta_5 D) D_5(s); & \begin{bmatrix} f_m \\ g_m \end{bmatrix} &= \sum_{n=-\infty}^{\infty} K_{n+m}(\beta_6 D) \begin{bmatrix} A_6(s) \\ B_6(s) \end{bmatrix}; & \begin{bmatrix} h_m \\ i_m \end{bmatrix} \\ &= \sum_{n=-\infty}^{\infty} K_{n+m}(\beta_7 D) \begin{bmatrix} A_7(s) \\ B_7(s) \end{bmatrix}. \end{aligned}$$

4. The relations between dynamic response and potentials

In polar coordinates, the displacement-potentials and stress-potentials and pore water pressure-potentials relations of saturated soil can be expressed as.

$$\bar{u}_r = \frac{\partial \bar{\varphi}_1}{\partial r} + \frac{1}{r} \frac{\partial \bar{\varphi}_1}{\partial \theta}, \quad \bar{u}_\theta = \frac{1}{r} \frac{\partial \bar{\varphi}_1}{\partial r} - \frac{\partial \bar{\varphi}_1}{\partial \theta}, \quad \bar{w}_r = \frac{\partial \bar{\varphi}_2}{\partial r} + \frac{1}{r} \frac{\partial \bar{\varphi}_2}{\partial \theta} \quad (17a)$$

$$\frac{\bar{\sigma}_r}{G_s} = (\lambda_s^* + 2) \frac{\partial^2 \bar{\varphi}_1}{\partial r^2} + \lambda_s^* \frac{\partial^2 \bar{\varphi}_1}{\partial \theta^2} + 2 \frac{\partial^2 \bar{\varphi}_1}{\partial r \partial \theta} + \alpha^2 M^* \nabla^2 \bar{\varphi}_1 + \alpha M^* \nabla^2 \bar{\varphi}_2 \quad (17b)$$

$$\frac{\bar{\sigma}_\theta}{G_s} = (\lambda_s^* + 2) \frac{\partial^2 \bar{\varphi}_1}{\partial \theta^2} + \lambda_s^* \frac{\partial^2 \bar{\varphi}_1}{\partial r^2} + 2 \frac{\partial^2 \bar{\varphi}_1}{\partial r \partial \theta} + \alpha^2 M^* \nabla^2 \bar{\varphi}_1 + \alpha M^* \nabla^2 \bar{\varphi}_2 \quad (17c)$$

$$\frac{\bar{\sigma}_{r\theta}}{G_s} = 2 \frac{\partial^2 \bar{\varphi}_1}{\partial r \partial \theta} + \frac{\partial^2 \bar{\varphi}_1}{\partial \theta^2} - \frac{\partial^2 \bar{\varphi}_1}{\partial r^2}, \quad \frac{\bar{\sigma}_f}{G_s} = -\alpha M^* \nabla^2 \bar{\varphi}_1 - M^* \nabla^2 \bar{\varphi}_2 \quad (17d)$$

The displacement-potentials and stress-potentials relations of the lining can be written in the following forms:

$$\bar{u}_r = \frac{\partial \bar{\varphi}}{\partial r} + \frac{1}{r} \frac{\partial \bar{\varphi}}{\partial \theta}, \quad \bar{u}_\theta = \frac{1}{r} \frac{\partial \bar{\varphi}}{\partial r} - \frac{\partial \bar{\varphi}}{\partial \theta} \quad (18a)$$

$$\begin{aligned} \frac{\bar{\sigma}_r}{G} &= 2 \left(\frac{\partial^2 \bar{\varphi}}{\partial r^2} + \frac{\partial^2 \bar{\psi}}{\partial r \partial \theta} \right) + \lambda^* \nabla^2 \bar{\varphi}, & \frac{\bar{\sigma}_\theta}{G} &= 2 \left(\frac{\partial^2 \bar{\varphi}}{\partial \theta^2} - \frac{\partial^2 \bar{\psi}}{\partial r \partial \theta} \right) + \lambda^* \nabla^2 \bar{\varphi}, \\ \frac{\bar{\sigma}_{r\theta}}{G} &= 2 \frac{\partial^2 \bar{\varphi}}{\partial r \partial \theta} + \frac{\partial^2 \bar{\psi}}{\partial \theta^2} - \frac{\partial^2 \bar{\psi}}{\partial r^2} \end{aligned} \quad (18b)$$

5. Boundary conditions in polar coordinate

Assuming that the saturated soil and the lining structure are completely continuous at the interface as shown in Fig. 1, the boundary conditions in $r_1=a_1$ can be expressed as:

$$\bar{u}_r^S = \bar{u}_r^L, \quad \bar{\sigma}_r^S = \bar{\sigma}_r^L \quad (19)$$

The displacement of the fluid relative to the solid equals to 0, that is:

$$\bar{w}_r^S = 0 \quad (20)$$

The stress of the inner surface lining ($r_1=a_2$) can be expressed as:

$$\bar{\sigma}_r^L = \frac{p_0}{s} \quad (21)$$

When $r_2=a_3$

$$\bar{\sigma}_r^S = 0, \quad \bar{\sigma}_f^S = 0 \quad (22)$$

Table 1
Model parameters.

n_f	ρ_L^*	ρ_s^*	ρ^*	α	M^*	λ^*	λ_s^*	ρ_m	G^*	G_s^*	b^*
0.3	1.5	1.2	0.6	0.98	20	100	2	3.5	100	0.005	100

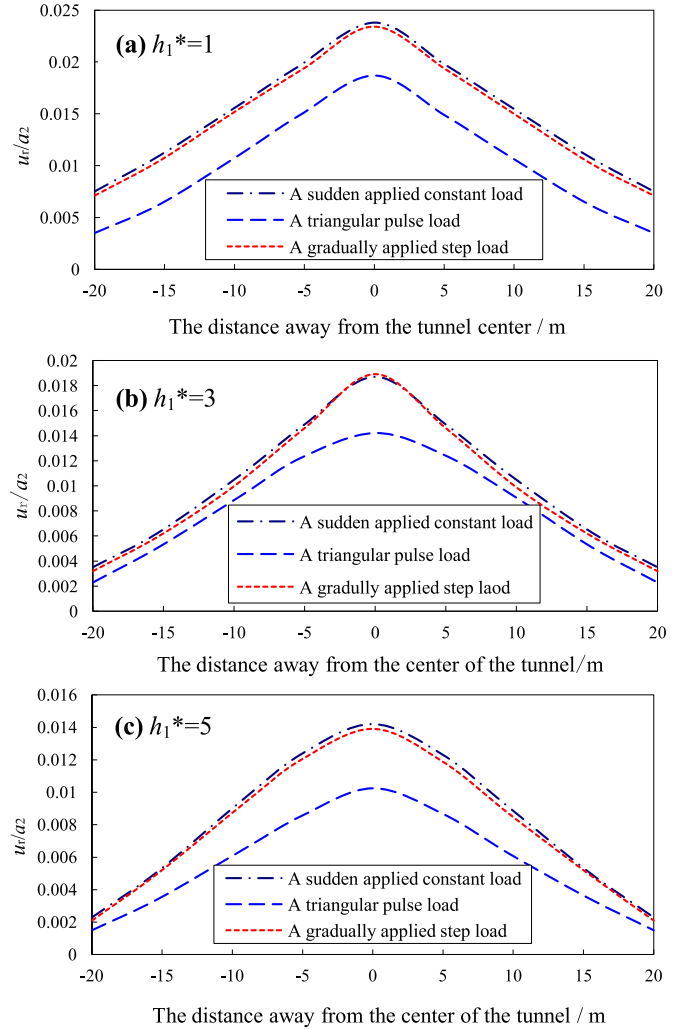


Fig. 2. Peak values of ground displacement at the different buried depths of tunnel.

where the superscripts *S* and *L* denote the variable quantities of saturated soil and the lining, respectively.

Substituting the potential function Eq. (16) into potential functions Eqs. (17) and (18), then substituting into boundary conditions Eq. (19), and properly limited to $n=12$, the undetermined parameters in Eq. (16) can be obtained.

6. The effect of buried depth on dynamic response of the tunnel

In order to analyze the effect of buried depth on dynamic response of the tunnel, the depth can be set as $h_1^* = h_1/a_2 = 1.0, 3.0, 5.0$. Other calculating parameters are given in Table 1 [1].

Under three types transient loads, the peak values of ground vertical displacement of tunnel at different buried depths are shown as Fig. 2(a), (b) and (c).

It can be seen that the peak value of ground vertical displacement significantly decreases with the increase of buried depth. The peak value of displacement reaches to maximum in the tunnel center. In addition, the peak values for a suddenly applied constant load and a

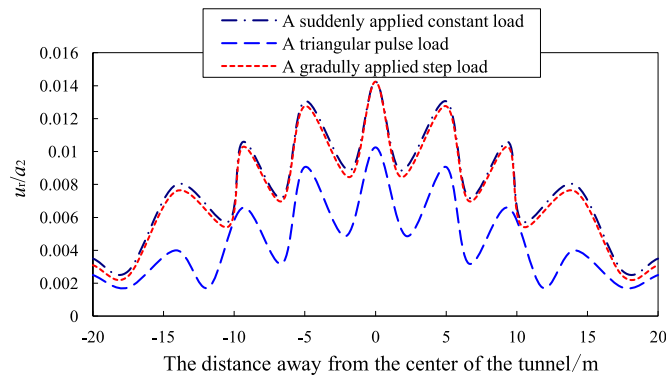


Fig. 3. Amplitude of ground displacement of the tunnel at $h_1^*=5$ and $t^*=1$.

gradually applied step load are very close. Furthermore, both values are much higher than that induced by a triangular pulse load.

As shown in Fig. 3, the amplitude of ground displacement reaches its maximum in the center of the tunnel and gradually reduces outwardly. The amplitude of ground displacements induced by a suddenly applied constant load is identical to that of a gradually applied step load and much greater than that under a triangular pulse load.

It has been observed that results corresponding to a gradually applied step load are almost equal to the ones under a constant load. In view of this, the solutions corresponding to a gradually applied load are not presented here for sake of brevity.

Fig. 4(a) and (b) give the displacement contour of saturated soil at $h_1^*=5$, $t^*=1$ induced by a suddenly applied constant and a triangular pulse load respectively. As shown in Fig. 4(a) and (b), the displacement contour in saturated soil shows a heart shape because the displacement above the tunnel presents the maximum value. Compared with Fig. 4(a), the displacement contour induced by a suddenly applied constant load in Fig. 4(b) is much closer to a heart shape, which indicates that the displacement just over the tunnel is much higher than that induced by a triangular load.

The hoop stresses (σ_θ/G_s) of the lining induced by a suddenly applied constant load in half-space and full-space are presented in Fig. 5(a) and (b), respectively. As shown in Fig. 5(a) for half-space, the hoop stress distribution is far from uniform in the inner surface of the lining. The maximum and the minimum hoop stress values are at the top and bottom of the tunnel respectively. While in full-space (deeply buried tunnel), the hoop stress is distributed symmetrically and only decreases with the thickness of the tunnel. Moreover, the hoop stress in the half-space is greater than that in full space.

Fig. 6(a) and (b) show the pore pressure distribution at the interface between the soil and the lining for $h_1^*=1$ at $t^*=1$ and $t^*=3$ corresponding to a suddenly applied constant load and a triangular pulse load. It

can be seen that pore pressure is minimal directly above the tunnel on the surface between the soil and the lining and maximal right below the tunnel. The pore pressure just above the tunnel decays to 0 rapidly with the radial direction to the ground, while the pore pressure right below the tunnel decreases gradually. The pore pressure induced by a triangular pulse load indicates obvious vibration compared with that induced by a suddenly constant load. The minimum value of the pore pressure occurs not only over the tunnel but also on the incline of both sides of the tunnel.

7. Conclusions

The main results of this study are summarized as follows:

- (1) The peak values of vertical ground displacements tend to be smaller with increasing the buried depth of the tunnel. The maximum peak value appears along the center line of the tunnel. The peak values and amplitude induced by a suddenly applied constant load and a gradually applied step load are similar to each other and far greater than that induced by a triangular pulse load. The amplitude of ground displacement reaches the maximum value in the center of the tunnel and gradually reduces outwardly.
- (2) The displacement contour in saturated soil shows a heart shape because the displacement above the tunnel is at its maximum. Assuming the buried depth value is infinite, the displacement contour should be a circle. Displacement contour induced by a suddenly applied constant load is much closer to a heart shape. The displacement gradient is greater right over the lining of the tunnel.
- (3) The hoop stress distribution is far from uniform in the inner surface of the lining. The maximum and the minimum hoop stress values are at the top and bottom of the tunnel respectively. While in full-space (deeply buried tunnel), hoop stress presents symmetric distribution and only decreases with the thickness of the tunnel. Moreover the hoop stress in the half-space is greater than that in full space.
- (4) The pore pressure right above the tunnel on the interface between the soil and the lining possesses minimum value and the maximum one is right below the tunnel. The pore pressure induced by a triangular pulse load indicates evident vibration compared with that induced by a suddenly constant load. The minimum value for the pore pressure occurs not only over the tunnel but also on the incline of both sides of the tunnel.

Acknowledgements

The research was supported by Program for Scientific Research Innovation Team of Qingdao Binhai University.

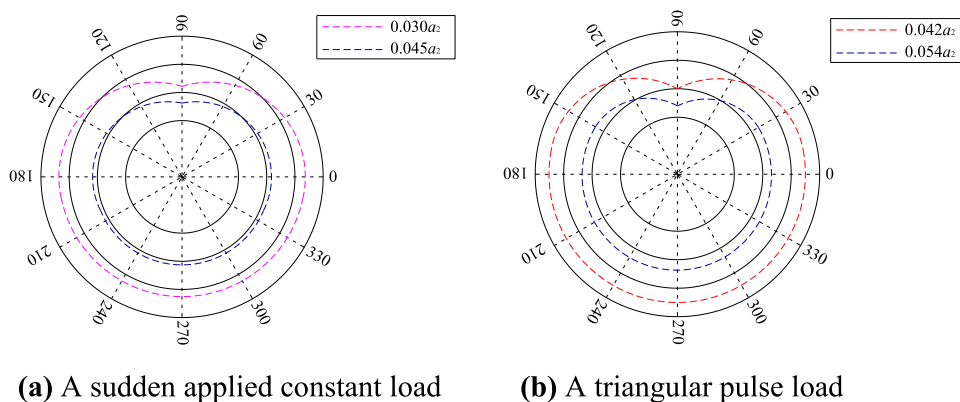


Fig. 4. Displacement contour in saturated soil at $h_1^*=5$ and $t^*=1$.

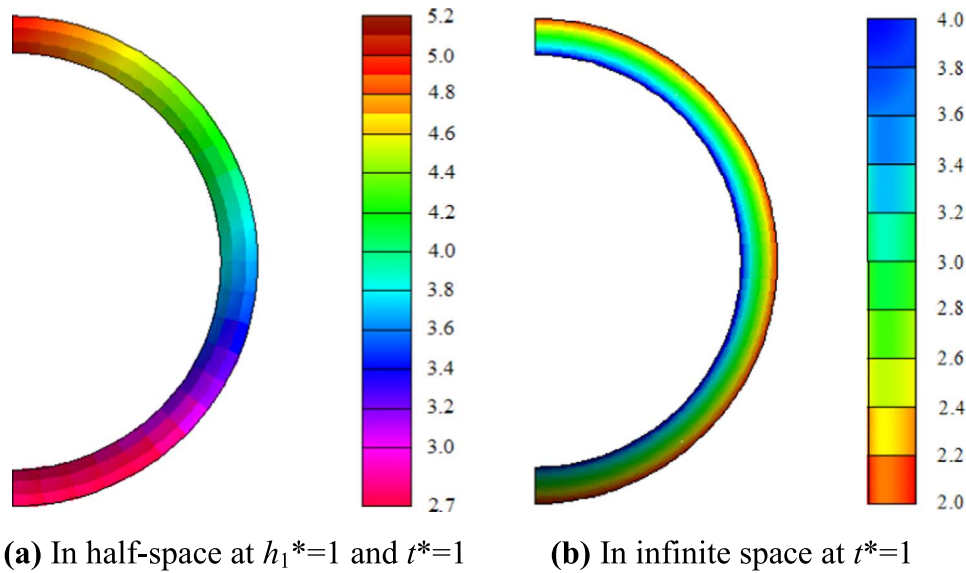


Fig. 5. The hoop stress (σ_θ/G_s) of the tunnel.

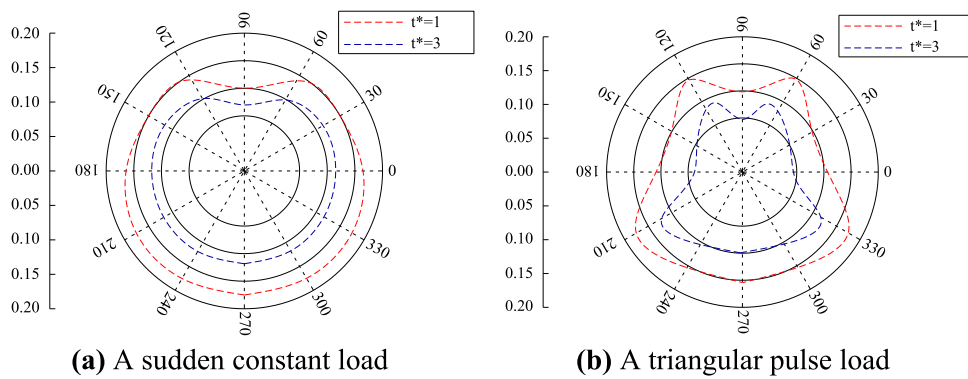


Fig. 6. The pore pressure distribution at the interface between the soil and the lining for $h_1^*=1$ at $t^*=1$ and $t^*=3$.

References

[1] Senjuntichai T, Rajapakse R. Transient response of a circular cavity in a poroelastic medium. *Int J Numer Anal Methods Geomech* 1993;17(6):357–83.

[2] Kattis SE, Beskos DE, Cheng AHD. 2D dynamic response of unlined and lined tunnels in poroelastic soil to harmonic body waves. *Earthq Eng Struct Dyn* 2003;32(1):97–110.

[3] Xie K, Liu G, Shi Z. Dynamic response of partially sealed circular tunnel in viscoelastic saturated soil. *Soil Dyn Earthq Eng* 2004;24(12):1003–11.

[4] Osinov VA. Blast-induced waves in soil around a tunnel. *Arch Appl Mech* 2011;81(5):543–59.

[5] Gao M, Wang Y, Gao GY, Yang J. An analytical solution for the transient response of a cylindrical lined cavity in a poroelastic medium. *Soil Dyn Earthq Eng* 2013;46(1):30–40.

[6] Wang Y, Gao GY, Yang J, Song J. The influence of the degree of saturation on dynamic response of a cylindrical lined cavity in a nearly saturated medium. *Soil Dyn Earthq Eng* 2015;71(8):27–30.

[7] Gao M, Zhang JY, Chen QS, Gao GY, Yang J, Li DY. An exact solution for three-dimensional (3D) dynamic response of a cylindrical lined tunnel in saturated soil to an internal blast load. *Soil Dyn Earthq Eng* 2016;90:32–7.

[8] Davis CA, Lee VW, Bardet JP. Transverse response of underground cavities and pipes to incident SV waves. *Earthq Eng Struct Dyn* 2001;30(3):383–410.